Available online at www.sciencedirect.com
ScienceDirect
Journal of the European Ceramic Society 28 (2008) 1737–1748
www.elsevier.com/locate/jeurceramsoc

Dehydration of $Ca_3Al_2(SiO_4)_y(OH)_{4(3-y)}$ $(0<y<0.176)$ studied by neutron thermodiffractometry

J.M. Rivas-Mercury [a], P. Pena [b,*], A.H. de Aza [b], X. Turrillas [c,1]

[a] *Centro Federal de Educão Tecnológica do Maranhão, CEP 65025-001 São Luís, MA, Brazil*
[b] *Instituto de Cerámica y Vidrio, CSIC, C/. Kelsen, 5, 28049 Cantoblanco, Madrid, Spain*
[c] *E. Torroja Institute for Construction Sciences (IETcc), CSIC, C/. Serrano Galvache, 4, 28033 Madrid, Spain*

Received 23 August 2007; received in revised form 18 December 2007; accepted 20 December 2007
Available online 19 March 2008

Abstract

Hydrogarnet ($Ca_{12}Al_2(OH)_{12}$) and katoite of composition $Ca_3Al_2(SiO_4)_{0.176}(OH)_{11.3}$ were obtained by hydration of tricalcium aluminium oxide, and for katoite synthesis, by addition of amorphous silica. The thermal dehydration was monitored *in situ*, by neutron thermodiffractometry, from room temperature to 700 °C at atmospheric pressure and at a heating rate of 2 °C/min. On heating, powder neutron diffraction patterns were collected every 300 s. Cell parameters were fitted by the Pawley method.

Hydrogarnet decomposed to yield $Ca_{12}Al_{14}O_{32}(OH)\cdot mH_2O$ and $Ca(OH)_2$ that eventually transformed to CaO. For katoite, phases of formula $Ca_{12}Al_{14-y}Si_yO_{32}(O,OH)_{1+y/2}$ related to mayenite were formed. Complementary annealing experiments, for 10 h, at higher temperatures and subsequent quenching lead to the formation of mayenite and traces of Ca_3SiO_5. Thermogravimetric curves were in agreement with the thermodiffractometry experiments.

Also, neutron diffraction data allowed to measure thermal expansion coefficients, at atmospheric pressure, between 25 and 250 °C for hydrogarnet and katoite: $1.89\times10^{-5}\pm0.09$ and $1.63\times10^{-5}\pm0.07\,°C^{-1}$, respectively.

Keywords: Thermal treatment; Neutron powder diffraction; X-ray methods; Thermal expansion; Calcium aluminates; Refractories

1. Introduction

Novel slip cast refractory materials – of strategic interest in many high-temperature industrial processes – are composed of coarse, medium and fine size fractions of various chemical and mineralogical compositions (Al_2O_3, $MgAl_2O_4$, $Al_6Si_2O_{13}$, SiC) with low additions of calcium aluminate cements (low cement castables (LCCs)) and variable additions of ultra fine active rheological agents such as silica fume, activated alumina and other small grain size additives.[1–3] The main role of silica fume is improving the rheology of the refractory concrete mix for better pumping and stability. Silica fume is widely used in LCCs and when combined with admixtures a system with low water demand can be achieved. Decreased water demand generally translates to lower porosity levels and improved strength development.

During hydration, of calcium aluminate cements, calcium and aluminium ionic species are produced which in the presence of silica fume precipitates katoite ($Ca_3Al_2(SiO_4)_y(OH)_{12-4y}$ $(0<y<0.33)$).[4] The hydration and dehydration of calcium aluminium oxides–silica fume mixtures have been little studied and are of great technological interest to find the most appropriate protocol conditions for the start up (hydration and dehydration) of a furnace concrete lining.

Our recent paper[5] reports work conducted *in situ* using neutron thermodiffraction on the dehydration of a pure an fully hydrated $CaAl_2O_4$ (hydrogarnet ($Ca_3Al_2(OH)_{12}$)/gibbsite ($Al(OH)_3$) mixture with a 1:4 molar ratio) in the temperature range 25–1300 °C. However, the dehydration of $Ca_3Al_2(OH)_{12}$ and $Ca_3Al_2(SiO_4)_y(OH)_{12-4y}$–silica fume mixtures has never been examined *in situ* by neutron thermodiffractometry (NTD). It is quite clear that understanding the dehydration of

* Corresponding author. Tel.: +34 91 735 58 40; fax: +34 91 735 58 43.
E-mail address: ppena@icv.csic.es (P. Pena).
[1] Also at European Synchrotron Radiation Facility (ESRF), BP 220, F-38043 Grenoble Cédex, France.

0955-2219/$ – see front matter © 2008 Published by Elsevier Ltd.
doi:10.1016/j.jeurceramsoc.2007.12.038

$Ca_3Al_2(SiO_4)_y(OH)_{12-4y}$ in the presence of amorphous silica is one of the main challenges in monolithic refractories.

For the present work, the experiments were conducted in fully hydrated mixtures of synthetic tricalcium aluminium oxide with and without silica fume, because the other components present in the castables—although important from a mechanical point of view—are chemically inactive at temperatures lower than 800 °C. So the coarse particles of castables were not added for two reasons: their chemical activity in the dehydration is negligible and they would interfere in the characterization by diffraction techniques.

To follow, in real time, the dehydration reactions, conventional thermal analysis techniques (differential thermal analysis, thermogravimetry) have been used, but these techniques by themselves cannot help to identify the reaction products or the transient phases that result from each thermal event. Therefore, although it is possible to spot the temperatures at which the reactions happen, they do not provide a precise indication of the solid phases present.

On the other hand, conventional methods of analysis require the reaction process to be abruptly interrupted, hence introducing an external interference. This procedure makes this approach less reliable. That is why diffraction methods, such as NTD, have been used also to identify phases formed and disappeared as the temperature raises.

The present work deals with the dehydration of both $Ca_3Al_2(OH)_{12}$ (hydrogarnet) and $Ca_3Al_2(SiO_4)_y(OH)_{12-4y}$ (katoite)–amorphous silica mixtures by NTD, on heating from room temperature to 700 °C. The analysis of these data has allowed determining the changes that occur with temperature at atmospheric pressure. The formation of various short-lived crystalline phases along the dehydration process like $Ca_{12}Al_{14-y}Si_yO_{32}(O,OH)_{1+y/2}$, $Ca(OH)_2$ and CaO were observed. The mean (linear) thermal expansion coefficients for the hydrogarnet and katoite are calculated in the temperature range 25–250 °C.

2. Experimental

2.1. Starting materials

Chemicals used were calcium carbonate ($CaCO_3$, Merck, Darmstadt, Germany), silica fume (Elkem Microsilica® from Elkem Materials, Pittsburgh, PA, USA)—98% reactive amorphous SiO_2 (150 nm diameter spheres) and amorphous aluminium hydroxide hydrate, $Al(OH)_3{\cdot}xH_2O$ (Aldrich, Milwaukee, WI, USA). Its precise composition was determined, by gravimetry, to be $Al(OH)_3{\cdot}0.949H_2O$.

2.2. Synthesis

To obtain $Ca_3Al_2O_6$ a stoichiometric mixture of $Al(OH)_3{\cdot}0.949H_2O$ and $CaCO_3$ powders were intimately mixed in an attrition mill using balls of zirconia partially stabilized with yttria in isopropanol, Then, were dried, isostatically pressed at 100 MPa and heated in platinum crucibles at 1300 °C for 10 h.

The samples were heated twice with an intermediate grinding to ensure homogeneity.

Finally, the product was examined by X-ray diffraction; the patterns only showed the reflections corresponding to $Ca_3Al_2O_6$. Preparation details regarding mechanism, time and temperature of synthesis are reported elsewhere.[6]

The hydrated specimens were obtained by mixing in water (in a water/solid ratio of 2) synthetic polycrystalline $Ca_3Al_2O_6$ with different amounts of amorphous silica to get nominal compositions of $Ca_3Al_2(SiO_4)_y(OH)_{12-4y}$ with $y=0$ and 1.7 hereafter referred to hydrogarnet and katoite. The stoichiometry of the hydrated products is given by the equations:

$$Ca_3Al_2O_6 + 6H_2O \rightarrow Ca_3Al_2(OH)_{12} \quad (1)$$

$$Ca_3Al_2O_6 + 2.4SiO_2 + 6-2yH_2O \rightarrow Ca_3Al_2(SiO_4)_y(OH)_{12-4y} + 2.4-ySiO_2 \quad (2)$$

The slurries were placed in teflon containers and kept, tightly closed, at 65 °C for three periods of 24 h, with intermediate milling processes.

2.3. Thermal analysis

Thermogravimetric analysis studies (STA 409, Netzsch, Germany) were conducted, on compacted samples, at a constant heating rate of 2 °C/min up to 1300 °C, in air, using Pt crucibles. Constant heating rate dilatometric studies (CHD) were conducted on a dilatometer (Setsys 16/18, Setaram, France) with alumina support on 20 mm long specimens on isostatically cold pressed compacts (50 MPa) at the same heating rate of 2 °C/min and up to 1300 °C, too. Additional isothermal treatments were performed in an electric furnace/Super-Kanthal, 1700 °C, Switzerland) at temperatures from 500 to 900 °C programming 2 °C/min ramps for both heating and cooling.

2.4. X-ray diffraction

X-ray diffraction was carried out with Cu Kα radiation in a powder diffraction (Siemens D-5000, Kristalloflex, Germany) with a secondary curved graphite monochromator working at 40 kV and 30 mA. NIST silicon powder (SRM 640c) was used as internal standard. Patterns were recorded from 10° to 130° (2Θ) in 0.03° steps, counting 25 s/step on specimens rotating at 15 min. Adequate slits were used to get optimal data for Rietveld refinement method.

2.5. Neutron diffraction

The high-temperature powder neutron diffraction experiments were carried out at the Institute Laue-Langevin (ILL) Grenoble, France, in Instrument D1B ($\lambda = 0.25227$ nm). A furnace was employed to reach temperatures up to 700 °C. The heating element, a vanadium cylinder, induced a constant temperature area of several centimetres along its axis. The temperature was continuously recorded and controlled by two chromel–alumel thermocouples (±5 °C accuracy) located next

to the heating element. Approximately 5 g of polycrystalline specimen lightly compacted were introduced into a quartz cylindrical tube of 10 mm diameter and 800 mm height, that was kept open to atmosphere during the entire experiment. This way, a uniform heat distribution in the whole sample was assured. Diffraction patterns were accumulated every 300 s on heating at a rate of 2 °C/min. These acquisition conditions imply a 10 °C temperature resolution for each pattern.

Powder neutron diffraction experiments at room temperature were carried out at the HRPT (High-Resolution Powder Diffractometer for Thermal Neutrons) instrument of the Swiss Spallation Neutron Source (SINQ) in the Paul Scherrer Institute (PSI) (Villigen, Switzerland). Data were collected in high intensity mode with $\lambda = 0.18857$ nm in the (2Θ) interval 2.45–163°, with a step/size of 0.05°. In these series of experiments, 5 g portions of sample were inserted into a cylindrical stainless steel tube of 10 mm internal diameter and 60 mm in height. Diffraction patterns were accumulated during approximately one hour to obtain 10^6 monitor counts.

2.6. Data analysis

General plotting of experimental data was carried out with the help of the commercial package Origin.[7] The visualization of data, under the form of 3D plots and contour maps, was made with the help of a commercial package, NOeSYS.[8]

In some cases free energy of reactions had to be calculated. This was done with the help of Outokumpu HSC,[9] a computing package that permits to calculate thermodynamic magnitudes thanks to an exhaustive database including enthalpy, entropy and heat capacity values for many chemical compounds.

X-ray and neutron diffraction data collected at room temperature were analysed by Rietveld method using Fullprof.[10] Neutron diffraction patterns from instrument D1B and X-ray diffraction data from the specimens annealed at higher temperatures were studied with the help of the commercial package Materials Studio[11]; cell parameters and crystallite size (for X-ray data) were refined with the method of Pawley.[12] The actual implementation used by Materials Studio is a variant[13] of the Pawley method to perform a peak shape, background, and lattice parameter refinement for an experimental powder pattern. As in the original Pawley method, the Bragg intensities are treated as refinable parameters.

To estimate the crystallite broadening the Scherrer equation was used where the full width at half maximum (FWHM) in 2θ is taken in consideration according to:

$$\Delta(2\theta)_a = 180\lambda/(\pi L_a \cos\theta)$$

where λ is the wavelength and L_a is the crystallite size, expressed in angstroms along the direction a. To compute crystallite sizes, the instrumental broadening of the diffractometer was measured with the help of a NIST Standard Reference Material: LaB_6 (SRM 660a) of known particle size distribution. The standard deviation for crystallite size is relative large since the residual stress broadening contribution was not taken in account. For the refinements the parameters related to instrumental broadening were kept fixed and it was assumed that the extra

Table 1
Phases identified in hydrated samples by XRD, TEM-EDS and NMR obtained at room temperature

Hydration reaction	Hydrated phases identified by XRD, TEM-EDS and NMR	T/t (°C)/(h)	XRD data for katoite by Rietveld analysis					
			Lattice parameter (Å)	Rwp	R_B	R_F	Occupancy of silicon	H
1	$Ca_3Al_2(OH)_{12}$	65/168	12.5748 ± 0.0004	2.99	9.07	6.43	0.0	12.0
2	$Ca_3Al_2(SiO_4)_{0.2}(OH)_{11.3}$, amorphous	65/168	12.529 ± 0.001	8.6	2.4	2.9	0.176 ± 0.002	11.3 ± 0.5

The cell parameters (in Å) and the statistical indicators of the Rietveld refinement are shown. For katoite the refinement was simultaneous with neutron and X-ray data. The figures are shown until the last certain digit. Amorphous phase = Amorphous.

broadening of diffraction peaks was solely due to crystallite size effects.

3. Results and discussion

3.1. Characterization of samples

The hydrated powders, according to the data obtained by X-ray diffraction, TEM and NMR, consisted of $Ca_3Al_2(OH)_{12}$[14] when no silica fume was added. When added, $Ca_3Al_2(SiO_4)_y(OH)_{12-4y}$ with unreacted amorphous silica was observed.[4]

Diffraction refinements of both samples, at room temperature, were made applying the Rietveld method, following the strategy and recommendations of McCusker et al.[15] using FULLPROF. Refinement details regarding structural model, number of phases included in the refinement and the type and number of parameters refined are reported elsewhere.[4,16] In Table 1 the more significant results obtained by X-ray diffraction, NMR and TEM, at room temperature, are shown.[14]

3.2. Thermal analysis

The thermograms (TGA and DTA curves) of pure and Si-containing samples, recorded at a constant heating rate of 2 °C/min are shown in Figs. 1(a) and 2(a), respectively. $Ca_3Al_2(OH)_{12}$ specimen losses 29.6% of its mass, in two stages; first 22.0% and then 7.2%. The first one with a minimum at

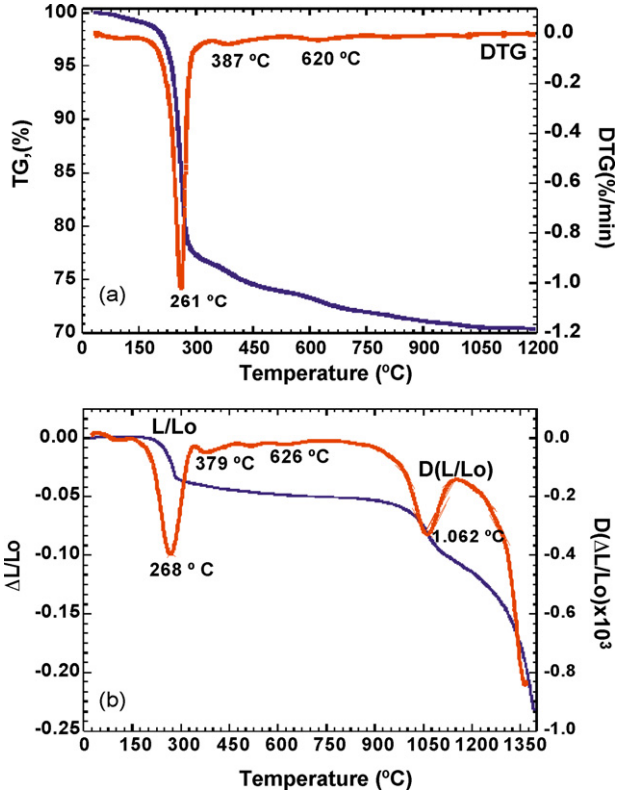

Fig. 1. Thermal analysis for synthetic hydrogarnet with a constant heating rate of 2 °C/min. (a) TGA and DTA curves. (b) Dilatometric curve and its derivative of a green compact specimen.

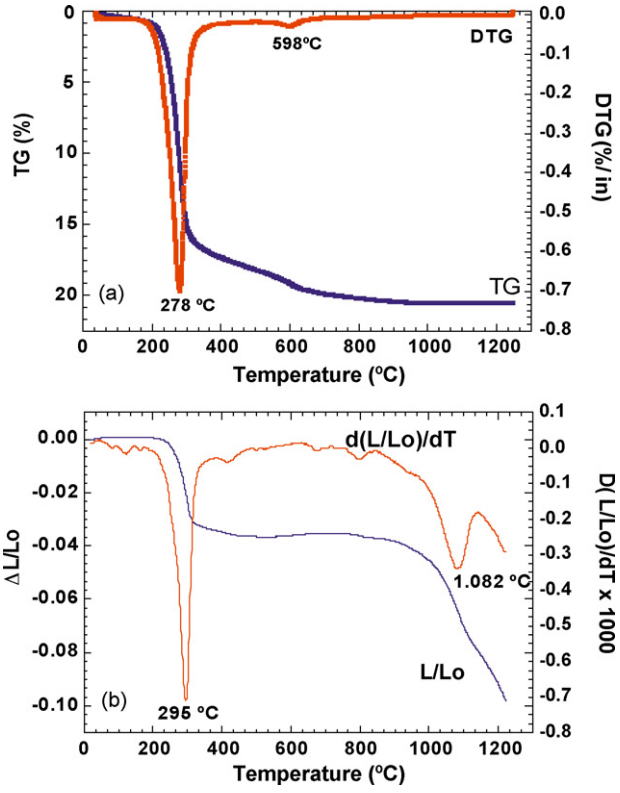

Fig. 2. Thermal analysis for katoite with a constant heating rate of 2 °C/min. (a) TGA and DTA curves. (b) Dilatometric curve and its derivative of a green compact specimen.

261 °C can be easily assigned to $Ca_3Al_2(OH)_{12}$ dehydration and the other effect in the 387–620 °C interval to a new H_2O release most likely related to the decomposition of calcium hydroxide ($Ca(OH)_2$).

$Ca_3Al_2(SiO_4)_y(OH)_{12-4y}$ plus amorphous silica mixture shows a total weight loss of 21.0% (Fig. 2(a)). This sample dehydroxilates between 210 and 350 °C losing 17.6% of its original mass with a maximum rate loss at 278 °C. After this first effect, still there is a progressive loss with no well-defined inflexion points. Clearly, around 598 °C there is an event that seems to be corroborated by the DTA curve but cannot be correlated to a particular reaction. The most obvious one would be the dehydration of $Ca(OH)_2$ to yield CaO. However, as it will be discussed later, other diffraction experimental results rule out this possibility.

3.3. Dilatometry

The constant heating rate (CHR) dilatometry and derivative curve of a low compacted $Ca_3Al_2(OH)_{12}$ (hydrogarnet) sample has been represented in Fig. 1(b). This sample suffered two shrinkage effects: the first one of 5%, in the temperature range 210–325 °C, was attributed to the dehydration of hydrogarnet; the second one at 975 °C was attributed to the sintering of the dehydrated sample. An inflexion point, attributed to an expansive reaction, at 1062 °C was also observed.

Fig. 2(b) corresponds to the CHR and derivative curve of the low compacted sample of $Ca_3Al_2(SiO_4)_y(OH)_{12-4y}$ (katoite) plus amorphous silica. This sample shows two significant shrink-

age effects with maxima at 295 and 1082 °C. The first one corresponds to the dehydration of katoite, the second one to the starts of the sample shrinkage. The inflexion in the shrinkage curve at 1100 °C is due to an expansive process.

3.4. Neutron thermodiffractometry

The evolution in real time of hydrogarnet and katoite with temperature can be seen in the 3D diagrams of Figs. 3(a) and 4(a). To visualise events such as diffraction shifts or collapse of phases more precisely, a contour map in two dimensions was projected from the 3D plot (Figs. 3(b) and 4(b)). The existence of phase domains was highlighted by labelling their diffraction peaks. Both contour maps clearly show the dehydration of $Ca_3Al_2(OH)_{12}$ and $Ca_3Al_2(SiO_4)_y(OH)_{12-4y}$ at temperatures up to 300 °C. The formation of various short-lived or intermediate phases such as $Ca(OH)_2$ and $Ca_{12}Al_{14}O_{33}$ in the temperature ranges 300–540 and 300–700 °C was observed too. The presence

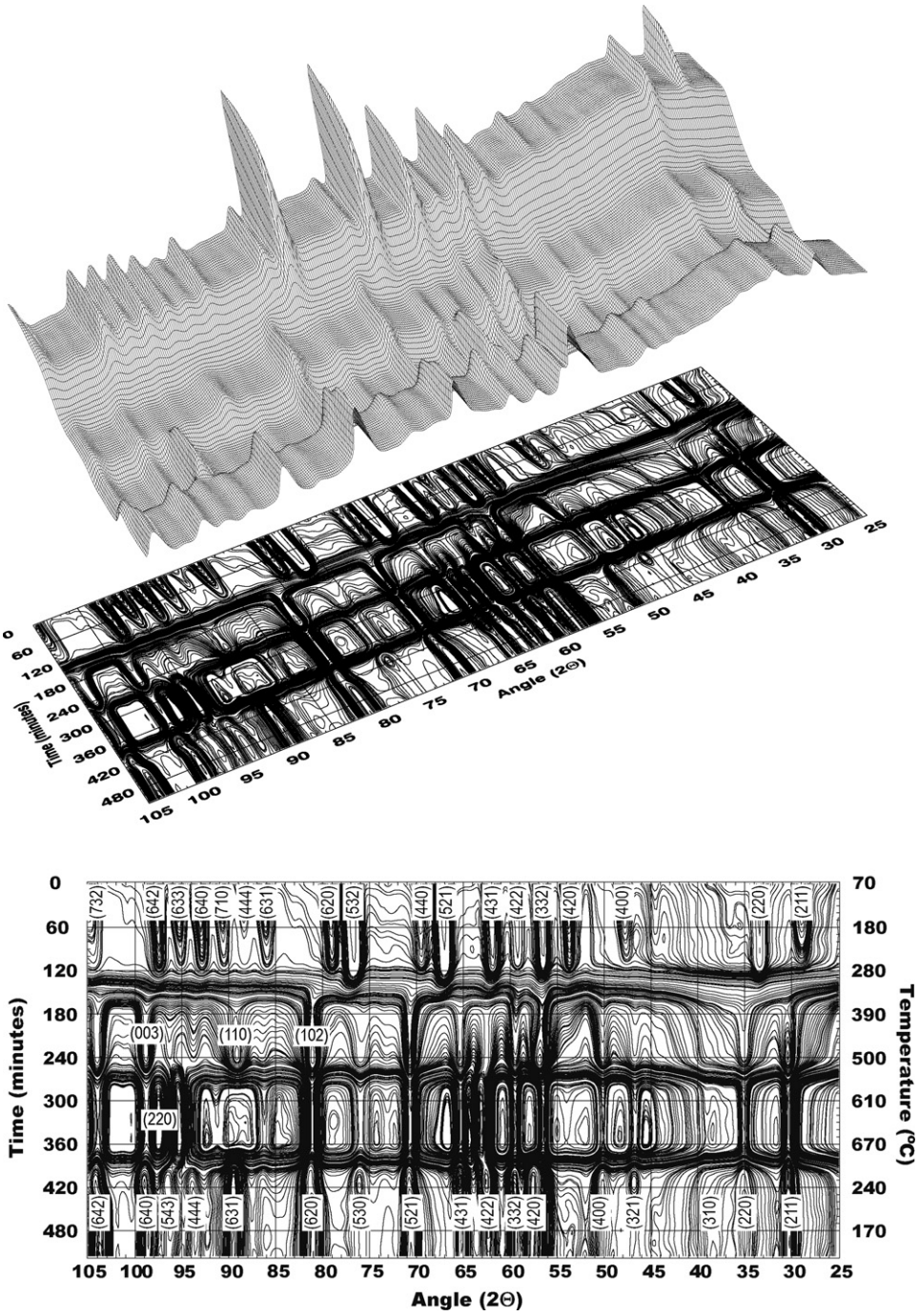

Fig. 3. Schematic representation of neutron diffraction patterns as topographic map for the dehydration of synthetic hydrogarnet: In abscissa, diffraction angle (2Θ), in left ordinate axis, the time in minutes and in right ordinate axis the corresponding temperature (°C). (a) Three-dimensional view in perspective with its two-dimensional projection as contour levels. (b) Two-dimensional projection highlighting with more detail the crystal phases and their corresponding (*h k l*) Miller indices. The first row represents hydrogarnet reflections, the second one, calcium hydroxide, the third one, calcium oxide and the last one, mayenite.

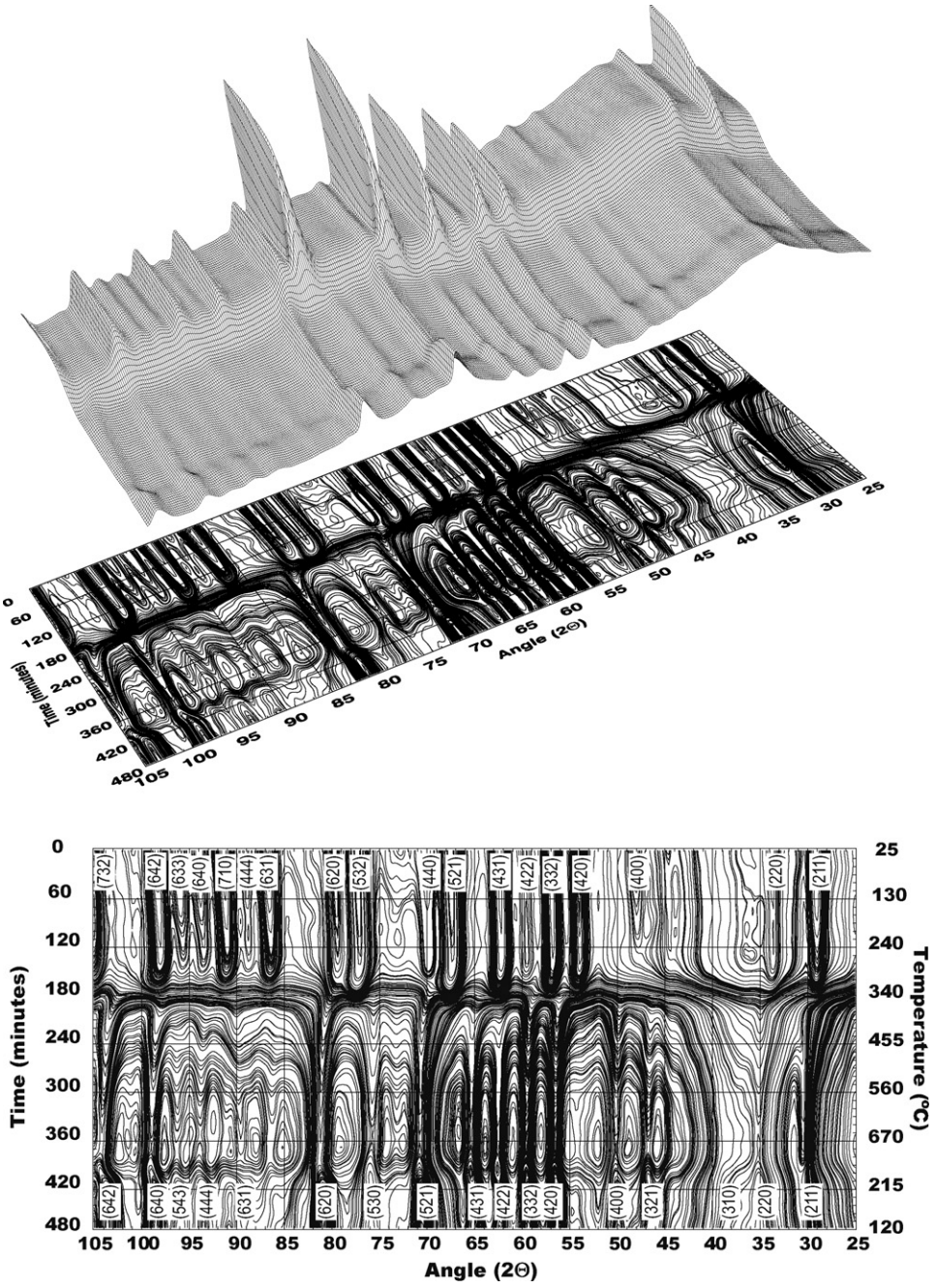

Fig. 4. Schematic representation of neutron diffraction patterns as topographic map for the dehydration of katoite. In abscissa, diffraction angle (2Θ), in left ordinate axis, the time in minutes and in right ordinate axis the corresponding temperature (°C). (a) Three-dimensional view in perspective with its two-dimensional projection as contour levels. (b) Two-dimensional projection highlighting with more details of the crystal phases and their corresponding ($h\,k\,l$) Miller indices. The first row represents katoite reflections, and the bottom one, silicon-substituted mayenite reflections.

of CaO has been observed at temperatures higher than 540 °C (Fig. 5). No evidence was offered for the formation of transition alumina. The progressive peaks shift to higher angles for katoite up to 250 °C suggests a hydrothermal reaction with remaining amorphous silica (Fig. 4(b)).

Because of the experimental conditions, the water released by the heating process was condensed in the top of the quartz tube; on cooling this water came down and reacted again with dehydrated powder forming katoite.

3.4.1. Variation of the predominant crystalline phases

Predominant phases have intense reflections that can be integrated (measurement of the area under the diffraction peak) and quantified. This is the case of $Ca_3Al_2(SiO_4)_{3-x}(OH)_{4x}$ (hydrogarnet and Si-hydrogarnet) and $Ca_{12}Al_{14}O_{33}$ (mayenite) For hydrogarnet and Si-hydrogarnet (katoite) the reflections (5 3 2 and 6 1 1) and for $Ca_{12}Al_{14}O_{33}$ the reflection (2 1 1) were selected. These reflections have been chosen to minimise the interference of peaks originated by other phases and by the

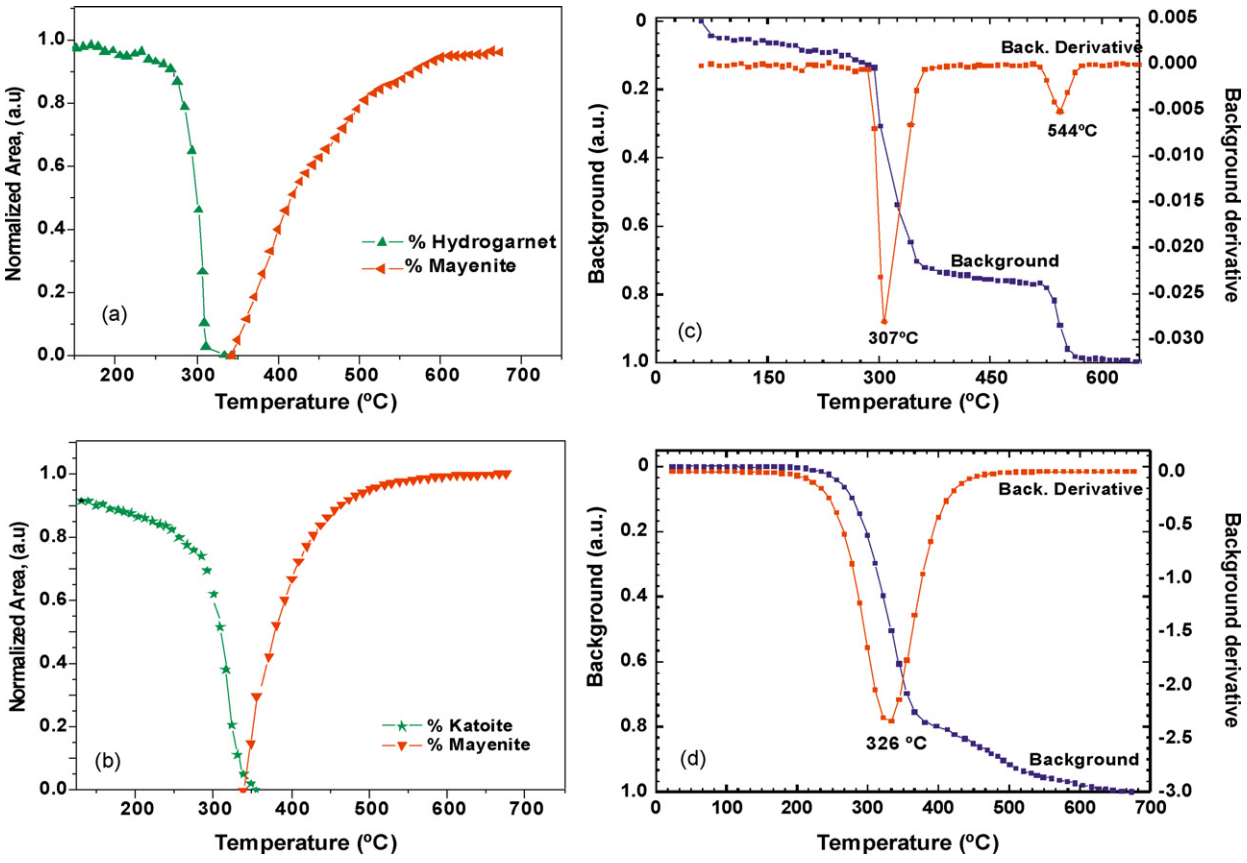

Fig. 5. (a) and (b) Integrated and normalized peaks of hydrogarnet, katoite and mayenite plotted against temperature. (a) Hydrogarnet sample and (b) katoite sample. See text for details. (c) and (d) The variation of the background of neutron diffraction data as a function of temperature has been represented for (c) hydrogarnet sample and (d) katoite sample. Their derivative curves are also represented.

experimental set up (see Figs. 3 and 4). The reaction progress was determined by normalising the peak intensities (i.e. $\alpha = 1$ when the $Ca_{12}Al_{14}O_{33}$ formation is completed, and 0 when dehydration is finished). Fig. 5(a) and (b) plots the extent of reactions, hydrogarnet and katoite decay (dehydration) and mayenite formation.

3.4.2. *Variation of NTD background*

In Fig. 5(c) and (d) the variation of the background of Neutron Diffraction data normalised to unity as a function of temperature has been represented for $Ca_3Al_2(OH)_{12}$ and $Ca_3Al_2(SiO_4)_y(OH)_{12-4y}$ plus silica fume samples. It is well known that there is a linear relationship between the content of hydrogen in any crystalline sample and the background level of their diffraction patterns related to the incoherent scattering of hydrogen. Therefore, the progressive diminution of background—that can be measured with some precision—reflects the OH content in hydrogarnet and katoite plus amorphous silica specimens.

The curve of hydrogarnet shows two maxima located at 307 and 543 °C corresponding to a water release of 78 and 22% of the total water content of sample. The first effect is due to partial dehydration of hydrogarnet to give $Ca(OH)_2$ and mayenite according to,

$$7Ca_3Al_2(OH)_{12} \rightarrow Ca_{12}Al_{14}O_{33} + 9Ca(OH)_2 + 33H_2O \quad (3)$$

This reaction is confirmed by diffraction. The second fall registered in the background is due to reaction,

$$9Ca(OH)_2 \rightarrow 9CaO + 9H_2O \quad (4)$$

Again this is confirmed by diffraction. These successive water departures imply a relation of 78.6 and 21.4% of total water loss that is in close agreement with those observed by ND: 78 and 22%. TG results of this work 22 and 7.2 wt% present small differences with the theoretical ones (22.4 and 6.2 wt%, respectively) and ND data; bearing in mind the water content of the samples. The minor discrepancies observed in the water release can be explained if is taken into account that the mayenite formed still contains in its crystal frame some water at temperatures as high as 600 °C. Assuming this hypothesis, we can suppose that the mayenite would form according the reaction,

$$7Ca_3Al_2(OH)_{12} \rightarrow Ca_{12}Al_{14}O_{32}(OH)\cdot mH_2O + 9Ca(OH)_2 + 33 - mH_2O \quad (5)$$

Nevertheless this is rather speculative, and counter arguments can easily be found, for example, the cell is not correspondingly larger.

More problematic is the interpretation of background profile for katoite, shown in Fig. 5(d). It is simpler and smoother, but only two things are clear. There is a maximum decomposition rate of katoite at 326 °C for the first step and then a progressive

fall which reflects a progressive evaporation of water. In the first step, approximately 76% of the total water is gone. The progressive fall or rather the absence of a well-defined decay after the first one corroborates the diffraction observation; calcium hydroxide and CaO are not formed. From these certain facts it is not possible to propose without doubt a reaction for the collapse of katoite. If it is assumed that during the dehydration, reactive silica in excess is involved in the formation of silicon-substituted mayenite. One possible path could be expressed by the equation,

$$4Ca_3Al_2(SiO_4)_{0.176}(OH)_{11.30} + 5.3SiO_2 \rightarrow Ca_{12}Al_8Si_6O_{32}(O, OH)_{1+y/2} + nH_2O \quad (6)$$

This way, the Ca/Al ratio would be maintained in the new phase and there would no need of introducing calcium hydroxide on the right side of the equation to balance it. It could be argued also that if silicon enters in smaller proportions the calcium in excess could react with silica to form amorphous hydrated calcium silicates. Again, with the present data it is not possible to answer this question.

3.4.3. Cell parameters of hydrogarnet and katoite

The neutron diffraction patterns collected on heating from 25° to 105° (in 2Θ) were refined, as explained earlier, with the help of Materials Studio[11] with the Pawley method. The temperature dependence of cell parameters for hydrogarnet and katoite from 25 to 250 °C is represented in Fig. 6.

These data can be fitted by linear least-squares analysis to a first-order polynomial to obtain for hydrogarnet:

$$a = 12.552 + 2.321 \times 10^{-4}T$$

and for katoite:

$$a = 12.506 + 2.047 \times 10^{-4}T$$

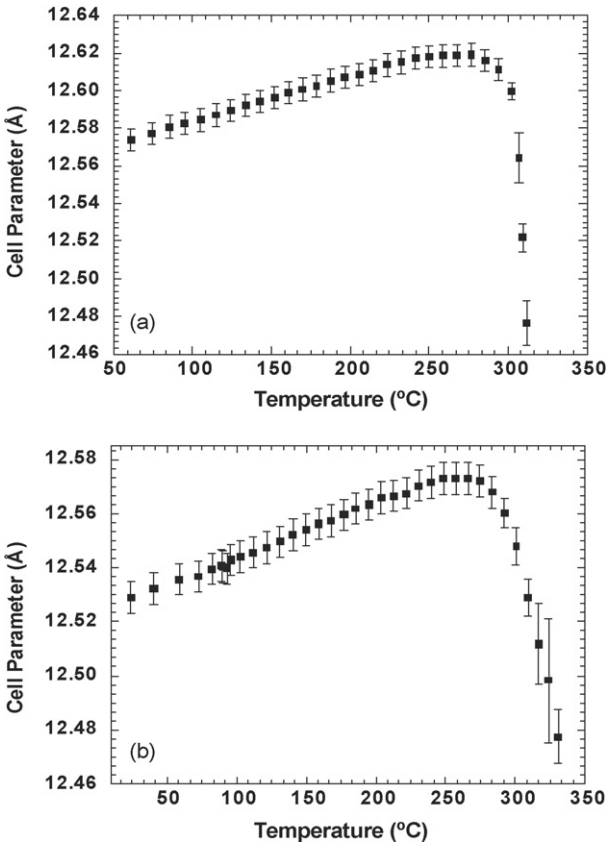

Fig. 6. The thermal expansion and eventual decay of (a) hydrogarnet and (b) katoite. The cell parameter is represented as a function of temperature. Error bars are also represented.

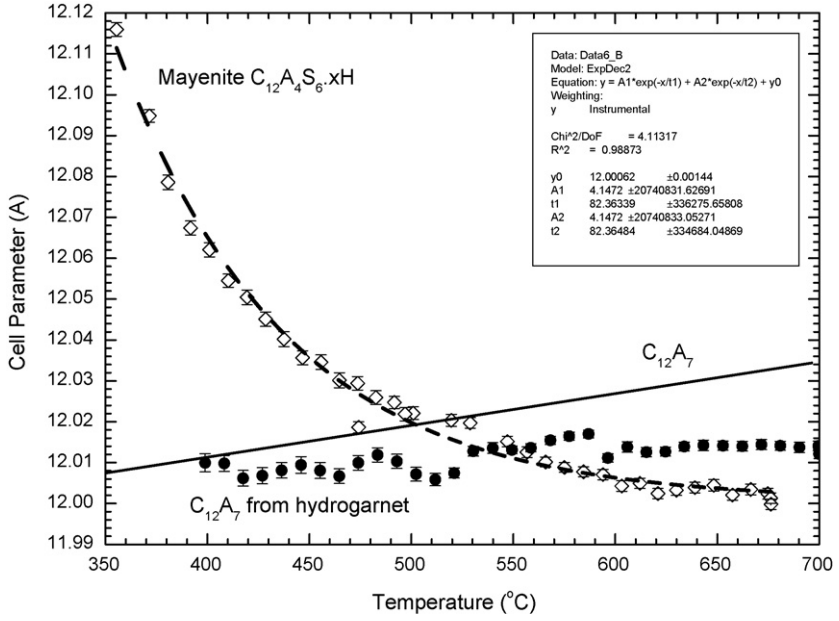

Fig. 7. Cell parameter variation for pure and Si-substituted mayenite as a function of temperature during NTD experiments compared with those measured in a specimen of mayenite, prepared at high temperature, from room temperature to 700 °C. Open lozenges stand for Si-substituted mayenite, bold circles for pure mayenite, and continuous line for mayenite synthesized at high temperature.

Table 2
Crystallographic description of a mayenite-like phase, $Ca_{12}Al_{14-x}Si_xO_{32}O_{1+x/2}$

Wyckoff	Atom	x	y	z	occ
24d	Ca	0.1034	0.0000	0.2500	1.00
16c	T1	−0.0183	−0.0183	−0.0183	1.00
12a	T2	0.3750	0.0000	0.2500	1.00
16c	O1	0.0593	0.0593	0.0593	1.00
48e	O2	0.0381	0.0543	0.6538	1.00
12b	O3	0.375	0.5000	0.2500	$(2+x)/12$

Space group I^-43d. Cell parameter $a = 12.001$ Å. T1 and T2 are generic names since the atoms present could be Al and/or Si.

The cell parameter variation up to 250 °C for both specimens was practically the same. This variation is continuous from 25 to 250 °C but at temperatures higher than 250 °C the parameter diminishes significantly due to the collapse of the crystalline structure of katoite, as it can be seen in Fig. 6 by the shrinkage of cell parameter. This effect might be due to the loss of groups OH^- inside the crystal structure during the decomposition.

3.4.4. Cell parameter variation of mayenite

The NTD data allowed measuring the cell parameters of both pure and Si-substituted mayenite. In Fig. 7 it is shown the evolution of them, together with the experimental thermal expansion profile of pure mayenite prepared at high temperature. These data were acquired in the same HRPT instrument mentioned in Section 2.5, but the complete experiment details are pending of publishing.

Before starting to discuss the main matter it is worth to look at the crystal structure of mayenite with some detail. Mayenite – described by Bartl[17] – is a relatively open structure and could be classified among the zeolitic ones.[18,19] Its ion crystal distribution can be found in Table 2. According to ref. [20] it is formed by a frame of two distinct types of small cation (Si^{4+} or Al^{3+}) tetrahedra in a 4:3 ratio. The T1 is coordinated by three O1 and one O2. T2 is surrounded by four O1. O1 always bridges between T1 and T2 but O2 is connected directly to a single T1. The shared O1 connect alternating T1 and T2 tetrahedra into approximately boat-shaped eight-membered rings. Sharing the remaining O1 serves to fuse the rings into a complete, rather open, three-dimensional structure. Linear units Ca–O3–Ca lie on twofold axes parallel to the unit-cell edges in the interstices of the aluminate framework in such a way as to allow Ca to achieve seven-coordination by contacts with four O1 and two O2 (Fig. 8).

The crucial point is that the position 24(d) occupied by O3 is scarcely populated and can accept a variety of large anionic species such as OH^-, O^{2-}, O_2^- or a combination of these species. The stability of the crystal structure hinges upon the $(Al,Si)_{14}O_{32}$ frame. The 24(d) site is used to counterbalance electric charge with bulky anionic species. Depending on the Al/Si ratio the 24(d) site will be more or less occupied.

Coming back to the cell parameter issue, now it is clear that having silicon in the mainframe, 24(d) will host a number of OH^- groups, that, as the temperature increases, will be replaced by anionic species without hydrogen – most likely O_2^- – and water will be released. This may happen in a gradual way and since the 24(d) site will lose population and the remaining anionic species are less bulky the volume cell will shrink accordingly. This is the most logical explanation for the apparent exponential decay of mayenite cell parameter observed in the neutron thermodiffraction experiment between 350 and 700 °C.

Contrarily, the specimen of hydrogarnet evolves in the expected way, i.e. the mayenite cell following an expansive trend. It does not match exactly the continuous line of Fig. 7 probably because it is badly crystalline and still might host some OH^- groups that at higher temperature leave the structure.

This is the same effect observed for the Si-substituted mayenite case although in a much lower extent.

3.5. Thermal treatments at constant temperature

To get some supplementary information about what happened at higher temperatures, both samples were thermally treated at constant temperatures of 500, 700 and 800 °C for periods of ten hours. These sets of data are not strictly comparable to the ones obtained dynamically; but they provide an idea about the crystalline phases present at a given temperature. Obviously, working this way, any transient or short-life phase that could be formed before reaching thermodynamic equilibrium would not be spotted, but still it is worth to conduct these experiments.

The heat treated specimens were analysed by X-ray diffraction at room temperature, X-ray diffraction patterns of the series of heat treated samples performed can be found in Figs. 9 and 10 (see Table 3). For hydrogarnet, as in the NTD experiments, mayenite and CaO were observed although at lower temperatures, which could be explained if it is considered that dynamic experiments could not reach equilibrium at every temperature recorded. Also, as the temperature was raised, $Ca_3Al_2O_6$

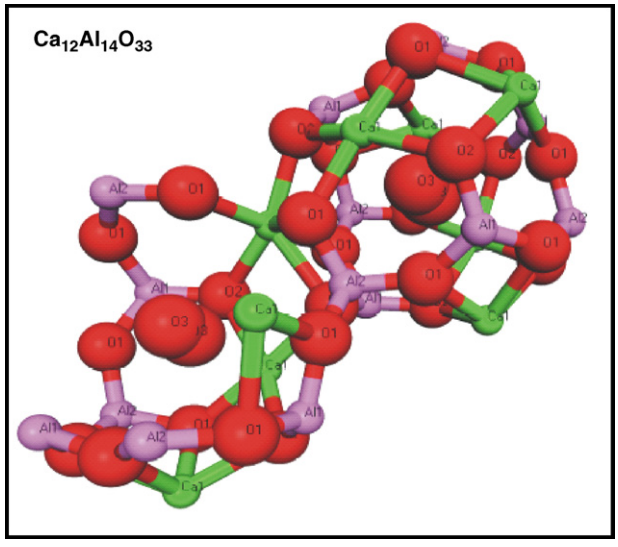

Fig. 8. View of the mayenite structure. The atoms are coloured as follows: calcium, green, aluminium, purple and oxygen, red. (For interpretation of the references to color in this figure legend, the reader is referred to the web version of the article.)

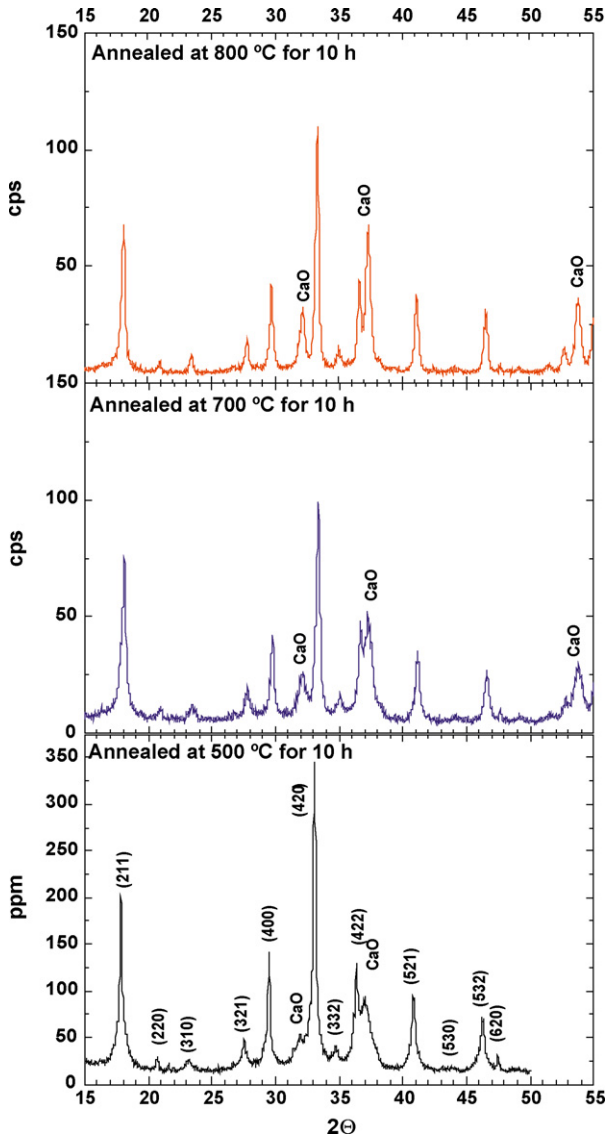

Fig. 9. X-ray diffraction patterns of hydrogarnet specimen heat-treated at 500, 700 and 800 °C for periods of 10 h. On the bottom the reflection corresponding to mayenite are labelled. Also the main diffraction peaks of CaO are indicated.

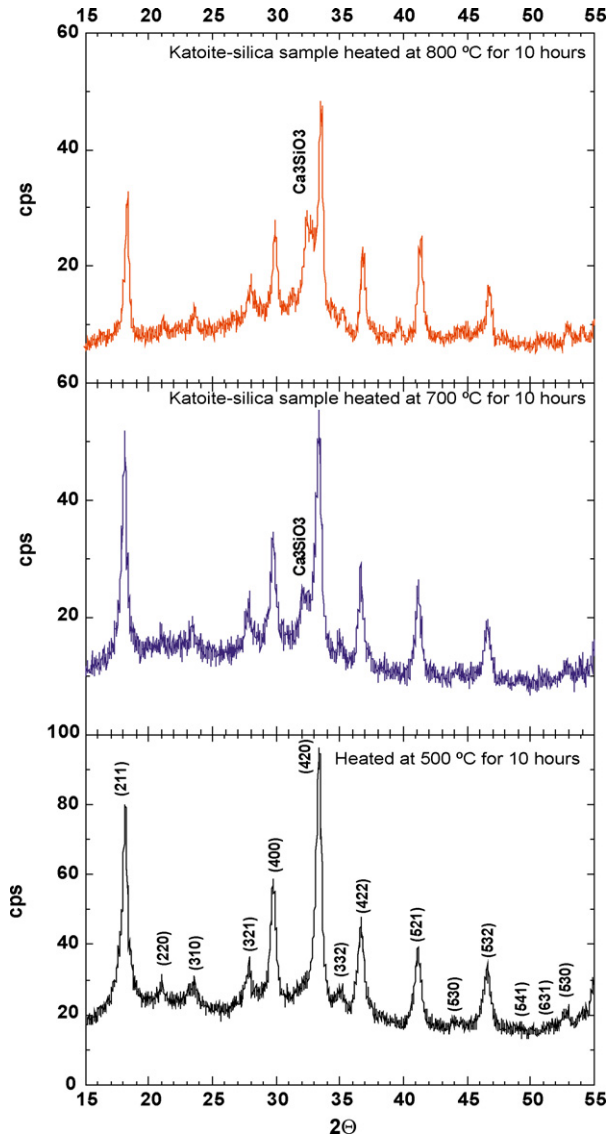

Fig. 10. X-ray diffraction patterns of katoite heat treated at 700 and 800 °C for periods of 10 h. As in Fig. 9, the reflections of mayenite-like phase are labelled on the bottom. At higher temperatures the peaks probably due to tricalcium silicate are indicated. Also is noticeable the relatively high background – compare to Fig. 9 – due to the presence of unreacted amorphous silicon oxide.

Table 3
Phases detected after annealing for periods of 10 h at the temperatures shown, at lower temperatures, cell parameters (until the last certain figure) and crystal sizes of pure and silicon-substituted mayenite phases were obtained using the Pawley method

Hydration reaction	*T*/*t* (°C)/(h)	Detected phases	Cell parameter (Å)	Rwp	Crystal size (Å)
	500/10	$Ca_{12}Al_{14}O_{33} + CaO(t)$	12.064 ± 0.001	11	220
	700/10	$Ca_{12}Al_{14}O_{33} + CaO$	12.018 ± 0.001	11	230
1	800/10	$Ca_{12}Al_{14}O_{33} + CaO$	12.028 ± 0.001	10	390
	1000/2	$Ca_{12}Al_{14}O_{33} + CaO + Ca_3Al_2O_6$	n.d.	n.d.	n.d.
	1250/2	$Ca_3Al_2O_6$	n.d.	n.d.	n.d.
	500/10	$Ca_{12}Al_{14-y}Si_yO_{33}$	12.036 ± 0.001	5.9	160
	700/10	$Ca_{12}Al_{14-y}Si_yO_{33} + Ca_3SiO_5(t)$	12.002 ± 0.001	8.0	180
2	800/10	$Ca_{12}Al_{14-y}Si_yO_{33} + Ca_3SiO_5(t)$	12.021 ± 0.001	9.2	270
	950/2	$Ca_{12}Al_{14-y}Si_yO_{33} + Ca_3SiO_5 + Ca_2Al_2SiO_7 + CaAl_2O_4(t)$	n.d.	n.d.	n.d.
	1250/2	$Ca_{12}Al_{14-y}Si_yO_{33} + Ca_3Al_2O_6 + Ca_2Al_2SiO_7$	n.d.	n.d.	n.d.

The statistical indicator Rwp is also displayed. (*t*) stands for traces. n.d. not determined.

appeared, and at the maximum temperature reached (1250 °C), was the only phase present (Table 3).

For katoite plus amorphous silica specimen, the formation of $Ca_{12}Al_{14-y}Si_yO_{33+y/2}$ and Ca_3SiO_5 were detected. The formation of this metastable silicon-substituted mayenite under hydrothermal conditions was reported by Fujita et al.[16,17] in relation to synthesis of new zeolite-related phases. However, phases such as transition aluminas were not detected. At higher temperatures, $Ca_3Al_2O_6$, mayenite and gehlenite were found.

Pawley refinements were made to measure the cell parameter and the crystalline size of $Ca_{12}Al_{14}O_{33}$ (mayenite) and $Ca_{12}Al_{14-y}Si_yO_{33+y/2}$ detected in the specimens heated in the range of temperatures between 500 and 800 °C. These values and the statistic indicators are shown in the Table 3. Whenever another crystal phase was present—apart mayenite—the Rwp indicators were not as good, since the presence of other crystal phases tampers the refinements.

Concerning the crystal structure of $Ca_{12}Al_{14-y}Si_yO_{33+y/2}$, in Section 3.4.3 the matter has been explained in some depth. The X-ray diffraction patterns cannot provide direct evidence of the actual substitution, more precisely; the relative intensities of reflections would not change upon partial replacement of Al^{3+} by Si^{4+}. The only way, indirect though, to undertake the problem is to measure cell parameters.

With these premises in mind the cell values listed in Table 3 have to be interpreted. For both $Ca_3Al_2(OH)_{12}$ (hydrogarnet) and $Ca_{12}Al_{14-y}Si_yO_{33+y/2}$ (katoite) plus silica fume specimens the trend observed is the same, but for katoite, the cell parameter lags behind because of the presence of smaller Si^{4+} ions. As the temperature is increased to 700 °C the cell, in both cases, shrinks. This effect could be attributed to departure of bulky OH^- groups from site 24d. The slight increase in cell volume observed at 800 °C is more difficult to explain. A few hypotheses could be proposed, but without further experimental evidence would be mere speculations. On the other hand, the progressive convergence of cell parameters, when temperature increases, would indicate a continuous departure of silicon from $Ca_{12}Al_{14-y}Si_yO_{33+y/2}$ to obtain an anhydrous phase less rich in silicon, and more Ca_3SiO_5.

To end the discussion of this section, the crystallite size evolution has to be commented. For both specimens it varies following the expected way, i.e. crystallites grow with temperature and the final size is still quite small. At 700 °C, the last temperature at which it was measured, the crystallinity is rather poor.

3.6. Mechanism of hydrogarnet dehydration

With the information provided in the previous sections it is possible to propose a mechanism for the events occurring up to 1250 °C in three steps.

- Above 300 °C hydrogarnet dehydrates producing mayenite $Ca_{12}Al_{14}O_{32}(OH)$ probably with some water trapped in its structure and portlandite $Ca(OH)_2$.
- Above 540 °C the dehydration of $Ca(OH)_2$ takes place to yield CaO.
- At temperatures higher than 1062 °C the expansive reaction of $Ca_3Al_2O_6$ formation occurs:

$$Ca_{12}Al_{14}O_{33} + 9CaO \rightarrow 7Ca_3Al_2O_6$$

Thermodynamic calculations indicate that at 1100 °C $\Delta G = -28$ kJ/mol, Therefore, it is understandable that at higher temperatures the only observed phase is $Ca_3Al_2O_6$.

3.7. Mechanism of katoite dehydration

In this case the dehydration reactions series is more complicated. Another three steps could be proposed.

- Above 250 °C and below 327 °C, katoite breaks apart. This is indicated by a decrease in the neutron diffraction background, a significant shift of katoite diffraction peaks towards higher angles, and by a thermal event at 280 °C in the TG, DTA and CHR curves. This effect could be attributed to a fast hydrothermal reaction of katoite with the unreacted ultrafine amorphous silica to get an unstable katoite phase with higher content of silicon.
- Above 350 °C, possibly, the hydrothermal process continues to yield this time $Ca_{12}Al_{14-y}Si_yO_{32}(OH)_{2+y}$, a silicon-substituted mayenite phase with an undetermined y value; it could be as large as 6.
- As the temperature is raised, the OH^- groups leave progressively the crystal structure as water, according to the equation,

$$Ca_{12}Al_{14-y}Si_yO_{32}(O, OH)_{1+y/2} \rightarrow Ca_{12}Al_{14-y}Si_yO_{32}O_{1+y/2} + nH_2O$$

Nevertheless, it is possible that this hypothetical extreme composition is not attained, and still some OH^- groups coexist with oxygen anions, or even O^{2-} species, according to Hosono andAbe[21] This mayenite phases were also observed by Fujita et al.[16,17,22] when preparing them by hydrothermal synthesis and subsequent heating at 800 °C.
- Above 500 °C the neutron *in situ* experiments did not reveal any other crystalline phase. However under other conditions, i.e. annealing the specimens at 500 °C, 700 °C and 800 °C in open atmosphere for periods of ten hours, Ca_3SiO_5 is formed. The reaction involved could be

$$Ca_{12}Al_{14-y}Si_yO_{33+y/2} \rightarrow Ca_{12}Al_{14}O_{33} + nCa_3SiO_5 + mSiO_2$$

This is just a simplified hypothesis; the crystal chemistry of mayenite being so rich, other more complex compositions could exist, since the site 24d could be populated by various anionic species, as it has been explained earlier.
- At 950 °C and above gehlenite, $Ca_2Al_2SiO_7$, is formed. The remaining silicon-substituted mayenite continues to break apart and at 1250 °C only gehlenite, $Ca_3Al_2O_6$ and $Ca_{12}Al_{14}O_{33}$ remain, which means that thermodynamic equilibrium has not been attained since the equilibrium phases at $T < 1265$ °C are $CaSiO_3$, $Ca_2Al_2SiO_7$ and $CaAl_2Si_2O_8$.[23]

4. Conclusions

The *in situ* evolution of hydrogarnet and katoite–amorphous silica mixtures has been studied by neutron diffractometry with a 10 °C resolution up to 700 °C. These data combined to other techniques such as DTA-TG, CHD and XRD have allowed determining the dehydration mechanism of both phases.

It has been possible to establish that the dehydration occurs in successive stages: dehydration of hydrogarnet and katoite above 250 °C and direct nucleation of mayenite and $Ca(OH)_2$ phases between 300 and 500 °C.

When amorphous silica was present the formation of a mayenite phase with some silicon substituting aluminium was observed. Neutron thermodiffractometry revealed a progressive loss of water manifested by a remarkable shrinking of its cell parameter of almost 10% from 300 to 650 °C. Subsequent thermal treatments at higher temperatures revealed the presence of Ca_3SiO_5. And finally above 800 °C the formation of gehlenite also was detected.

The cell parameters of hydrogarnet and katoite have been measured from 25 to 350 °C and are practically linear, but at temperatures above 250 °C the cell parameter diminishes significantly due to the degradation of their crystal structure.

Acknowledgements

This research was supported by MCYT under the projects MAT-2003-08331-CO2-01 and MAT2006-12749-C02-01-02. We thank ILL for beam time granted (experiment number 5-25-83) and Dr. J. Campo for his assistance in collecting ND data. We also thank to Dr. D. Sheptyakov for experimental assistance in collecting the neutron diffraction data at SINQ (experiment number II/02 S-18).

References

1. Lee, W. E., Viera, W., Zang, S., Ahai, K. G., Sarpoolaky, H. and Parr, C., Castable refractory concretes. *Int. Mater. Rev.*, 2001, **46**(3), 145–167.
2. Rivas-Mercury, J. M., de Aza, A. H., Turrillas, X., Rodríguez, M. A. and Pena, P., Estudio por difracción de rayos X de la hidratación de mezclas de $CaAl_2O_4$-humo de sílice. *Bol. Soc. Esp. Ceram. Vidr.*, 2007, **46**(6), 280–288.
3. Rivas-Mercury, J. M., de Aza, A. H., Turrillas, X. and Pena, P., Calcium aluminate cements hydration. Part II: effect of silica and alumina additions. *Bol. Soc. Esp. Ceram. Vidr.*, 2003, **42**(6), 361–368.
4. Rivas-Mercury, J. M., Turrillas, X., de Aza, A. H. and Pena, P., Calcium aluminates hydration in presence of amorphous SiO_2 at temperatures below 90 °C. *J. Solid State Chem.*, 2006, **179**(10), 2988–2997.
5. Turrillas, X., Convert, P., Hansen, T., De Aza, A. H., Pena, P., Rodriguez, M. A. *et al.*, Dehydration of calcium aluminate hydrates investigated by neutron thermodiffractometry. In *Proceedings of the International Conference on Calcium Aluminate Cements*, ed. R. J. Mangabhai and F. P. Glasser. Edinburgh, 2001, pp. 517–531.
6. Rivas-Mercury, J. M., De Aza, A. H., Turrillas, X. and Pena, P., The synthesis mechanism of $Ca_3Al_2O_6$ from soft mechanochemically activated precursors studied by time-resolved neutron diffraction up to 1000 °C. *J. Solid State Chem.*, 2004, **177**, 866–874.
7. Program Origin Version 7.0. Microcal Software Inc., Northampton, MA, USA; 2004.
8. Program NOeSYS. Version 1.2. Research Systems Inc. (Kodak Company), Sterling, VA 20164, USA; 1998. http://www.rsinc.com/.
9. Outokumpu HSC Chemistry for Windows Version 1.10. Outokumpu Research Oy, Pori, Finland; 1993.
10. Rodríguez-Carvajal, J., In *Satellite Meeting on Powder Diffraction of the XV IUCr Congress, 127*, 1990.
11. Accelrys Materials Studio v. 4.0. Accelrys, Cambridge, CB4 0WN, UK; 2005.
12. Pawley, G. S., Unit-cell refinement from powder diffraction scans. *J. Appl. Cryst.*, 1981, **14**, 357.
13. Engel, G. E., Wilke, S., Harris, K. D. M. and Leusen, F. J. J., PowderSolve—a complete package for crystal structure solution from powder diffraction patterns. *J. Appl. Cryst.*, 1999, **32**, 1169–1179.
14. Larger, G. A., Armbruster, T. and Faber, J., Neutron and X-ray diffraction study of hydrogarnet $Ca_3Al_2(O_4H_4)_3$. *Am. Mineral.*, 1987, **72**, 756–765.
15. McCusker, L. B., Von Dreele, R., Cox, B., Louer, D. E. and Scardi, D. P., Rietveld refinement guidelines. *J. Appl. Crystallogr.*, 1999, **32**, 36–50.
16. Rivas Mercury, J. M., De Aza, A. H., Turrillas, X., Pena, P., Sobrados, I. and Sanz, J., Solid state ^{27}Al and ^{29}Si NMR investigation on Si-substituted hydrogarnets. *Acta Mater.*, 2007, **55**, 1183–1191.
17. Bartl, H. and Séller, T., Zur strukture des $12(CaO)(7(Al_2O_3)$. *Neues Jahrb Mineral Montas.*, 1970, 547–552.
18. Fujita, S., Suzuki, K., Ohkawa, M., Shibasaki, Y. and Mori, T., Reaction of hydrogrossular with hydrogen chloride gas at high temperature. *Chem. Mater.*, 2001, **13**(8), 2523–2527.
19. Fujita, S., Suzuki, K., Ohkawa, M., Mori, T., Iida, I., Miwa, Y. *et al.*, Oxidative destruction of hydrocarbons on a new zeolite-like crystal of $Ca_{12}Al_{10}Si_4O_{35}$ including $O_2(-)$ and $O_2(2-)$ radicals. *Chem. Mater.*, 2003, **15**(1), 255–263.
20. Fenq, Q. L., Glasser, F. P., Howie, R. A. and Lachowski, E. E., *Acta Crystalogr.*, 1988, **C44**, 589–590.
21. Hosono, H. and Abe, Y., Occurrence of superoxide radical ion in crystalline $12CaO{\cdot}7Al_2O_3$ prepared via solid-state reactions. *Inorg. Chem.*, 1987, **26**(8), 1192–1195.
22. Fujita, S., Ohkawa, M., Suzuki, K., Nakano, H., Mori, T. and Masuda, H., Controlling the quantity of radical oxygen occluded in a new aluminum silicate with nanopore. *Chem. Mater.*, 2003, **15**(26), 4879–4881.
23. Aramaki, S. and Roy, R., The mullite corundum boundary in the systems $MgO–Al_2O_3–SiO_2$ and $CaO–Al_2O_3–SiO_2$. *J. Am. Ceram. Soc.*, 1959, **42**(12), 644–645.